Lipids in Health and Disease

RESEARCH Open Access

SEC14L2 regulates the transport of cholesterol in non-small cell lung cancer through SCARB1

Qianhui Zhou[1], Dianwu Li[1], Yanchao Liang[1], Yunzhu Long[2*] and Yi Liu[1*]

Abstract

Background Inhibiting cholesterol metabolism has shown great potential in non-small cell lung cancer (NSCLC). However, the regulatory mechanism of the lipid metabolism key factor Sect. 14-like lipid binding 2 (SEC14L2) in NSCLC remains unclear. This study investigates the effects of differentially expressed genes related to cholesterol metabolism on the development of NSCLC.

Methods Cox regression and survival analysis were performed to screen cholesterol metabolism-related genes and predict survival prognosis in NSCLC patients. The proliferation and migration of NSCLC cells were assessed by CCK-8, EdU, colony formation and wound-healing assay. Cholesterol depletion and rescue trials were used to evaluate the effect of SEC14L2 on cholesterol transport in NSCLC cells. IF and Co-IP were used to analyze the targeting relationship between SEC14L2 and scavenger receptor class B member 1 (SCARB1).

Results SEC14L2 was a key gene related to prognosis in NSCLC patients and was highly expressed in A549 and Calu-1 cells. Subsequent studies demonstrated that knockdown of SEC14L2 significantly reduced the proliferation and migration of NSCLC cells, resulting in inhibited tumor growth. Furthermore, both in vitro and in vivo experiments indicated that SEC14L2 regulated cholesterol uptake. Silencing SEC14L2 partially counteracted the promotion of cholesterol content by MβCD-chol in A549 and Calu-1 cells. We then verified that there was a protein interaction between SEC14L2 and SCARB1.

Conclusion SEC14L2 promoted cholesterol uptake in NSCLC cells by up-regulating SCARB1 expression, thereby promoting NSCLC development.

Keywords SEC14L2, SCARB1, Cholesterol metabolism, NSCLC

Introduction

Lung cancer is the most common type of primary tumor, and it is estimated to be newly diagnosed in more than 2 million people each year, according to Global Cancer Statistics [1]. Among them, non-small cell lung cancer (NSCLC) accounts for 80-85%. The majority of patients with early NSCLC miss the best treatment opportunities due to the lack of clinical manifestations, so it still has a high mortality rate [2]. In addition, studies have shown that many cancer patients become overweight or obese due to excessive nutritional supplementation after diagnosis or successful treatment [3]. There is growing

*Correspondence:
Yunzhu Long
2863454482@qq.com
Yi Liu
hui648934631@126.com
[1]Department of Respiratory and Critical Care Medicine, Zhuzhou Central Hospital, No.116, Changjiang South Road, Tianyuan District, Zhuzhou 412000, Hunan, China
[2]Department of Infectious Diseases, Zhuzhou Central Hospital, No.116, Changjiang South Road, Tianyuan District, Zhuzhou 412000, Hunan, China

concern that inappropriate diets may have a significant impact on impairing treatment outcomes in cancer patients [4]. This implies that consuming large amounts of cholesterol may affect the survival of cancer patients.

Cholesterol serves as a critical component of lipids and is important for the proliferation and survival of cancer cells [5]. During the process of cancer cell proliferation, an excess of cholesterol is required to support rapid membrane biogenesis [6]. Cholesterol metabolism can generate tumor-promoting substances [7]. Regulating cholesterol metabolism may impact cancer cell proliferation [8]. Studies have shown that genes in the cholesterol-related pathways can predict the survival of NSCLC [9]. Alterations in the cholesterol biosynthesis pathway induce cell death in NSCLC [10]. The reduction of plasma membrane cholesterol contributes to enhanced anticancer activity in NSCLC [11]. Recent studies have shown that cholesterol depletion can reduce NSCLC adhesion, thereby regulating NSCLC cell metastasis [12]. Lung cancer accumulates cholesterol through local and distal lipid transport reprogramming, and interventions to eliminate cholesterol may offer a promising therapeutic strategy [13]. Therefore, we focused on the impact of differentially expressed genes associated with cholesterol metabolism on the development of NSCLC.

The SEC14p protein is the prototype of a family of eukaryotic proteins carrying the Sect. 14-lipid-binding domain and plays a role in lipid metabolism, signaling, and membrane transport [14]. Section 14-like lipid binding 2 (SEC14L2) is one of the members of the Sect. 14 family, which encodes lipid-binding proteins, including α-tocopherol transporter and contributes to vitamin E uptake [15]. Previous studies have demonstrated that hTAP1/ SEC14L2-mediated lipid exchange regulates the phosphorylation of tocopherol and phosphatidylinositol [14]. α-tocopherol and α-tocopherol phosphate induce VEGF expression through PI3Kγ/PKB and hTAP1/ SEC14L2 mediated lipid exchange [16]. These reports indicate that SEC14L2 is closely related to lipid exchange. Moreover, numerous studies have demonstrated that SEC14L2 is connected with the development of prostate cancer [17], liver cancer [18], breast cancer [19], and other cancers. Still, the regulatory mechanism of SEC14L2 in NSCLC is unclear.

STRING database showed that there might be a protein interaction between SEC14L2 and scavenger receptor class B member 1 (SCARB1). It has been suggested that SCARB1 plays an important role in cholesterol metabolism [20, 21]. In the study, we used NSCLC cell lines A549 and Calu-1 to construct in vitro and in vivo NSCLC models to investigate whether SEC14L2 regulates cholesterol metabolism and tumor growth by interacting with SCARB1.

Materials and methods

Source of data set

The gene set related to cholesterol metabolism was sourced from MSigDB. RNA-seq data and clinical information pertaining to NSCLC were obtained from the Cancer Genome Atlas (TCGA, https://portal.gdc.cancer.gov/) database. Additionally, the NSCLC GSE50081-related chip data set was downloaded from the Gene Expression Omnibus (GEO, https://www.ncbi.nlm.nih.gov/geo/) database. TCGA and GEO belong to public databases. The patients involved in the database have obtained ethical approval. Our study is based on open source data, so there are no ethical issues, and the Clinical Trial Number is not applicable.

Bioinformatics analysis

In terms of abs (logFC)>log2 (1.5) and significant $P<0.05$ was used as the screening condition for differential gene analysis, and the differentially expressed genes in the combined MsigDB and TCGA NSCLC data were screened out. To visualize the results, the "ggplot2" software package was utilized to generate a volcano plot, while the "heatmap" package was employed to create a heatmap illustrating the differential gene expression. Univariate Cox analysis was performed on the TCGA dataset to analyze the differentially expressed genes further. The forest map was drawn for genes with $p \leq 0.05$, and 5 prognostic-related genes were obtained. Survival analysis of these key genes was conducted using the "survival" package and the "survminer" package. Additionally, GSEA analysis was performed using clusterProfiler based on SEC14L2 related genes. The enrichment plot for GSEA analyses were generated using the "ggplot2" package in R software [22]. Prediction of a protein interaction between SEC14L2 and SCARB1 by the STRING database.

Cell culture and transfection

NSCLC cell lines A549 (AW-CCH011), Calu-1 (AW-CCH019), NCI-H1299 (AW-CCH038), HCC827 (AW-CCH208), NCI-H157 (AW-CCH102) and NCI-H358 (AW-CCH297) were obtained from Changsha Abiowell Biotechnology Co., LTD. Among, A549 cells were cultured in F12K medium supplemented with 10% fetal bovine serum (FBS, 10099141, Gibco, Grand Island, NY, USA) and 1% penicillin-streptomycin (AWH0529a, Abiowell). On the other hand, Calu-1 cells were cultured in F12K and McCOY's 5 A medium, supplemented with 10% FBS+1% penicillin-streptomycin.

Logarithmic cells were transfected using Lipofectamine 2000 (11668019, Invitrogen, Carlsbad, CA, USA) as described in the kit after cell adhesion. Cells were transfected or co-transfected with si-SEC14L2-1 (HG-shHO456571, HonorGene, 5'-AGGAAGGTGGAGAC CATCACCATAA-3'), si-SEC14L2-2 (HG-shHO456571,

HonorGene, 5'-GAGGCCTATGGAGAGTTTCTCTG CA-3'), si-SEC14L2-3 (HG-shHO456571, HonorGene, 5'-GAGGAAGGTGGAGACCATCACCATA-3'), si-SCARB1 (HG-shHO710270, HonorGene, 5'-GCCAA GAGAAATGCTATTTAT-3'), and oe-SCARB1 (HG-HO710270, HonorGene). Cells were transfected for 48 h before subsequent experiments were performed.

In order to assess SEC14L2 effects on cell proliferation and migration, and the regulatory relationship between SEC14L2 and SCARB1, A549 and Calu-1 cells were randomly assigned to Control, si-NC and si-SEC14L2 groups. To investigate the SEC14L2 regulation function of cholesterol transport, we randomly divided A549 and Calu-1 cells into MβCD-chol, MβCD-chol+si-NC and MβCD-chol+si-SEC14L2 groups. Additionally, A549 and Calu-1 cells were randomly divided into the MβCD-chol+si-NC, MβCD-chol+si-SCARB1, MβCD-chol+oe-NC and MβCD-chol+oe-SCARB1 groups, to verify whether SEC14L2 regulated cholesterol metabolism through SCARB1.

Real-time quantitative polymerase chain reaction (RT-qPCR)

According to the Total RNA Extraction (Trizol, 15596026, Thermo, Waltham, MA, USA) method specification, total RNA was extracted from tissues and cell culture. Then, the absorbance values of total RNA were measured by an ultraviolet spectrophotometer. The subsequent experiments will continue when the OD260/OD280 conforms to 1.8-2.0. β-actin was used as an internal standard control for mRNA in RT-qPCR. RT-qPCR was performed using the SYBR method in a Quantstudio1 (ABI, Foster, CA, USA). Primer sequences are shown in Table 1. Gene levels were analyzed by the $2^{-\Delta\Delta Ct}$ method.

Cell counting Kit-8 (CCK-8) assay

A549 and Calu-1 cell viability were detected by a CCK-8 kit (NU679, Tongren, Japan). In the logarithmic growth phase, the cells were seeded at a density of 5×10^3 cells/well in a 96-well plate, and 10 μL CCK8 was added to each well for the corresponding time. After continued incubation at 37℃ and 5% CO_2 for 4 h, the absorbance value at 450 nm was analyzed with a microplate reader (MB-530, HEALES, Shenzhen, China), and the mean value was taken as a bar graph.

Table 1 Primer sequences used in the study were listed

Targets	F (5'-3')	*R* (5'-3')
H-SEC14L2	GGCCATGCTCCGGAAGTT	AAGACGCTTC AGTGTTTCGG
H-SCARB1	TCACTTCCTCAACGCTGACC	TCCAATGCCT GCGACAGATT
H-β-actin	ACCCTGAAGTACCCCATCGAG	AGCACAGCCT GGATAGCAAC

Ethynyl-20-deoxyuridine (EdU) incorporation assay

A549 and Calu-1 cells were seeded in 96-well plates until normal growth. An EdU assay kit (C10310, RIBOBIO, Guangzhou, China) was utilized for the experiment. The EdU solution was diluted 1:1000 to prepare an appropriate 50 μM EdU medium. Subsequently, 100 μL EdU medium was added and incubated overnight. After discarding the medium, the cells underwent Apollo and DNA staining, followed by a wash with PBS for 5 min. Finally, cell proliferation was observed using a fluorescence microscope (AE31E, Motic, Xiamen, China).

Colony formation assay

Firstly, the cells were digested with 0.25% trypsin. These cells were then suspended with 10% FBS. Each group of cell suspensions was seeded at 200 cells per well in 6-well plates containing 1 mL culture medium to make the cells evenly dispersed and cultured for 2 weeks. Once the clones were observed, the cultures were terminated. To fix the cells, 1 mL of 4% paraformaldehyde was added, and the cells were allowed to incubate for 15 min. Subsequently, cells were stained with crystal violet for 30 min. After drying naturally, it was photographed for recording.

Wound-healing assay

Once the A549 or Calu-1 cells had completely adhered to the culture dish, the spear's tip was compared with the ruler and scratched vertically. After scratching, floating cells were removed, and serum-free McCoy's 5 A/MEM medium was added. The progress of cell healing was recorded by capturing photographs at 0 h, with three different fields of view captured at each time point. Images were captured at 24 h and 48 h time points during the cell culture process for documentation.

Transwell assay

A549 and Calu-1 cells were digested by trypsin and suspended in a serum-free culture medium. The cells with a density of 2×10^6/mL (100 μL/well) were inoculated into a Transwell chamber (3428, Corning, USA) coated with Matrigel matrix gel (356234, Biocoat, USA). Then culture medium containing 10% FBS was added to the lower chamber of the 24-well plate and incubated in a humidified atmosphere of 5% CO_2 at 37℃ for 4 h. After removing the chamber, cells were fixed with 4% paraformaldehyde for 20 min. After cells were stained for 5 min with crystal violet solution (G1062, Solarbio). Stained cells were observed and counted under a microscope.

Animal models

Referring to previous studies [23, 24], we purchased a total of 15 athymic BALB/c nude mice (4–6 weeks). These mice were randomly divided into three groups: Control, sh-NC, and sh-SEC14L2. Mice were anesthetized

after one week of adaptive feeding and then subcutaneously injected with A549 cells. The cell concentration was 5×10^6/mL, and 200 μL was injected. After 7 days, intratumoral injection of sh-NC and sh-SEC14L2 (1×10^{10} PFU/mouse, injected every 14 days) [25]. The growth of the transplanted tumors was then monitored, with neoplasia defined as tumors with a diameter≥0.5 cm. The following formula was used to calculate tumor volume: Tumor volume = (short axis × short axis × long axis) / 2. Tumor size was measured twice a week after tumor seeding. After 24 days, the tumors were photographed and harvested.

All experimental procedures and animal handling were performed with the approval of the Animal Care and Use Committee of the Second Xiangya Hospital, Central South University (Approval No. 2023867), in accordance with the National Institutes of Health Guide for the Care and Use of Laboratory Animals, and studies involving laboratory animals followed the ARRIVE guidelines.

All experimental procedures and animal handling were performed with the approval of the Animal Care and Use Committee of the Second Xiangya Hospital, Central South University (Approval No. 2023867), in accordance with the National Institutes of Health Guide for the Care and Use of Laboratory Animals, and studies involving laboratory animals follows the ARRIVE guidelines.

Immunohistochemistry (IHC)

Tumor specimens were collected from nude mice, fixed, dehydrated, and embedded in paraffin. The paraffin sections were subjected to baking at 60℃ for 12 h. After that, they were deparaffinized using xylene and dehydrated through an ethanol gradient. Antigen thermal repair was performed after dipping it in distilled water for 5 min. To inactivate the endogenous enzyme, 1% periodate was added. Then, the cells were incubated overnight at 4℃ with SEC14L2 (AWA12665, 1:200, Abiowell) and Ki67 (ab16667, 1:200, Abcam, Cambridge, MA, USA). After incubating with secondary antibodies, color development was terminated after 3,3'-Diaminobenzidine (DAB, ZLI-9018, ZSGB-BIO, Beijing, China) coloration for 1–5 min, followed by hematoxylin counterstaining for 5–10 min. Finally, it was dehydrated, transparent, and sealed. After capturing the image, it is analyzed with Image-Pro-Plus 6.0.

Western blot (WB) analysis

The cells and tissues in each group were rinsed with precooled PBS buffer and then added with RIPA lysate (AWB0136, Abiowell) to lyse them. After the protein concentration was measured using a BCA kit (AWB0104, Abiowell), the corresponding volume of protein was added to a 5×loading buffer (AWB0055, Abiowell) for mixing. Electrophoresis was terminated when bromophenol blue electrophoresis reached the bottom of the glue. The membrane transfer current was 300 mA, and the transfer time was adjusted for different antibodies. After the membrane was transferred, it was rinsed once in 1×PBST, and then the membrane was completely immersed in the blocking solution and shaken on the shaker for 90 min at room temperature. These primary antibodies were diluted with 1×PBST at a ratio: low-density lipoprotein receptor (LDLR, AWA49839, 1:1000, Abiowell), SCARB1 (ab217318, 1:2000, Abcam), ATP-binding cassette transporter A1 (ABCA1, AWA41977, 1:1000, Abiowell), β-actin (AWA80002, 1:5000, Abiowell). The membrane was incubated with the primary antibody overnight at 4℃. Finally, the membrane was incubated with ECL chemiluminescence solution (AWB0005, Abiowell) for 1 min and observed with a chemiluminescence imaging system (ChemiScope6100, Clinx Science Instruments, Shanghai, China).

Cholesterol depletion and rescue assay

Cells with a 70 to 80% fusion rate were subjected to cholesterol depletion. 1% methyl-β-cyclodextrin (MβCD) was added to DMEM for 30 min, followed by 20 μm pravastatin.

For cholesterol rescue experiments, after cholesterol depletion, cells were incubated with 100 μm soluble cholesterol-MβCD complex (MβCD-chol) for 1 h and 40 μm pravastatin was added to DMEM. When assays were completed, cells were lysed and subjected to immunoblotting. MβCD-chol was added to the culture medium to supplement cholesterol in cell growth at a final concentration of 10 μg mL^{-1}.

Cellular cholesterol extraction and quantification

To extract cellular cholesterol, we referred to the method described by Zheng et al. [26]. Firstly, chloroform, methanol, and 0.9% NaCl were used for the extraction process. Then, we spotted 5 μL of the extracted sample onto silica gel thin-layer chromatography plates. The plates were developed using a petroleum-ether ethyl-acetate mixture (1:2). Finally, we utilized ImageJ to quantify cholesterol content intensity.

Immunofluorescence (IF)

The slides were first fixed for 30 min. Subsequently, 0.3% Triton X-100 was used to permeate for 30 min. After washing, 5% BSA-PBS was applied to the block for 60 min. The primary antibody SCARB1 (Bsm-52283R, 1:50, Bioss, Beijing, China) was added and incubated overnight at 4℃. Next, the slides were incubated with HRP secondary antibody for 30 min and then reacted with TSA-520 fluorescent dye (AWI0688, Abiowell) for 10 min. At the end of the reaction, the previous round of antibody was eluted, and an endogenous

peroxidase-blocking agent was added. The cells were then blocked for 60 min. The primary antibody SEC14L2 (AWA12665, 1:50, Abiowell) was added and incubated overnight at 4℃. After incubation with HRP secondary antibody, TSA-570 fluorescent dye was added to the reaction for 10 min and then eluted. DAPI staining solution (AWI0429, Abiowell) was dropped and incubated for 10 min in the dark. Finally, they were observed by fluorescence microscopy.

Co-immunoprecipitation (Co-IP) analysis

The cells were rinsed using PBS and IP cell lysate (AWB0144, Abiowell). Total proteins were obtained by centrifugation of the lysate and subsequently incubated overnight with SCARB1 antibodies. 20 μL of Protein A/G agarose beads were added to capture antigen-antibody complexes, and the antigen-antibody mixture was incubated on a shaker at 4℃ for 2 h. After co-immunoprecipitation, the expressions of SEC14L2 and SCARB1 were detected using WB [27].

Statistical analysis

Statistical analysis was conducted using GraphPad Prism 8.0 software. Data were represented as mean ± standard deviation (SD). If the data followed a normal distribution, we performed pairwise comparisons between the two groups using the T-test. Comparisons between multiple groups were performed using the one-way or two-way analysis of variance, and then Tukey's multiple comparisons test was used. The level of significance was set at $P<0.05$.

Results

Cholesterol metabolism-related gene SEC14L2 predicted the prognosis of NSCLC patients

106 cholesterol metabolism genes were screened from the MsigDB database and combined with the TCGA NSCLC dataset for differential analysis. We visualized the differential expression of 35 candidate genes, including 5 differentially up-regulated genes and 30 differentially down-regulated genes, in the form of a volcano plot and heat map (Fig. 1A and B). To further screen the prognostic relevance of differentially expressed genes in NSCLC patients, we performed a univariate Cox analysis and drew the forest plot. Five genes were associated with the prognosis of NSCLC patients, among which VDAC1, MSMO1, SEC14L2 and PCSK9 were high-risk genes, and MYLIP was a low-risk gene (Fig. 1C). Previous studies showed that SEC14L2 was closely related to lipid exchange [14, 16]. Therefore, we selected SEC14L2 for subsequent analysis. Our study examined the SEC14L2 expression using RT-qPCR in six different cell lines: A549, Calu-1, NCI-H1299, HCC827, NCI-H157, and NCI-H358. Our results demonstrated that SEC14L2 expression was higher in A549 and Calu-1 cells (Fig. 1D). Consequently, A549 and Calu-1 cells were selected for subsequent in vitro experiments. Then, a single-gene survival analysis of SEC14L2 was performed by combining the TCGA dataset and the survival data of NSCLC patients from GEO (GSE50081) data. The results showed that the SEC14L2 low-expression group had a better prognosis than the high-expression group (Fig. 1E). Taken together, these findings suggested that SEC14L2 was a key gene affecting the prognosis of NSCLC patients.

The inhibition of SEC14L2 expression suppressed the proliferation and migration of A549 and Calu-1 cells

Subsequently, SEC4L2 expression was silenced in A549 and Calu-1 cells and target screening was performed. The results showed that si-SEC14L2-3 exhibited a lower expression level compared with si-SEC14L2-1 and si-SEC14L2-2 in A549 and Calu-1 cells (Fig. 2A and B). This result indicated that si-SEC14L2-3 had the best silencing effect, leading to its selection for the subsequent experiments. Following this, we detected the cell viability using the CCK-8 method. As illustrated in Fig. 2C, the cell viability of the si-SEC14L2 group was decreased compared with the si-NC group. To further assess cell proliferation, we conducted EdU and colony formation assays, which demonstrated a markedly lower proliferation rate in the si-SEC14L2 group compared with the si-NC group (Fig. 2D-F). The migration ability of A549 and Calu-1 cells was also assessed by the wound-healing and transwell assay, which revealed a significantly reduced migration ability in the si-SEC14L2 group as compared to the si-NC group (Fig. 2G and H). These results collectively indicated that inhibiting SEC14L2 expression could effectively inhibit the proliferation and migration activity of A549 and Calu-1 cells.

SEC14L2 promoted the development of NSCLC

To investigate the role of SEC14L2 in NSCLC development further, we performed in vivo tumor formation experiments in nude mice. The results revealed that the tumors' survival rate and volume were decreased in the sh-SEC14L2 group compared with the sh-NC group (Fig. 3A-C). IHC detection of the expression of SEC14L2 and Ki67 demonstrated a significant reduction in SEC14L2 and Ki67 expression levels in the sh-SEC14L2 group, indicating that the proliferation of tumor cells was significantly reduced after knocking down SEC14L2 (Fig. 3D). These findings suggested that SEC14L2 had the potential to promote tumor growth.

SEC14L2 targeted SCARB1 to regulate cholesterol uptake

Based on the TCGA database, we performed a GSEA analysis of functional pathways associated with SEC14L2

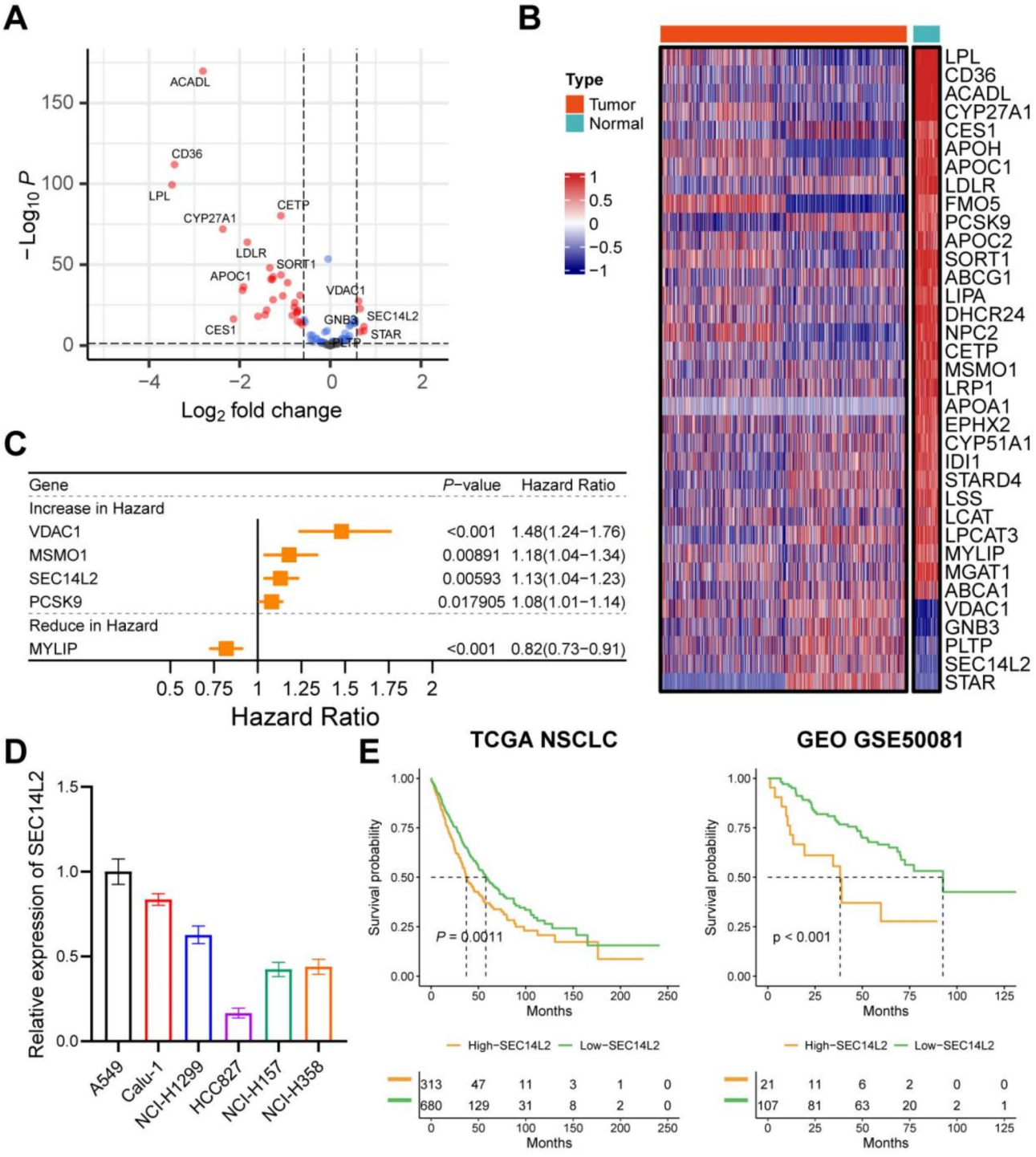

Fig. 1 Cholesterol metabolism-related gene SEC14L2 predicted the prognosis of NSCLC patients. (**A** and **B**) A volcano plot and heat map were used to visualize the differentially expressed genes related to cholesterol metabolism. (**C**) We employed univariate Cox analysis to assess the prognostic impact of these genes in NSCLC patients. (**D**) The expression of SEC14L2 in human NSCLC cell lines was detected using RT-qPCR. (**E**) The survival data from the TCGA datasets and GEO (GSE50081) data were combined to perform a single-gene survival analysis of SEC14L2 in NSCLC patients

gene expression. The GSEA analysis indicated a correlation between SEC14L2 and cholesterol metabolism (Fig. 4A). Further analysis through the online software STRING revealed the relationship between SEC14L2 and proteins related to cholesterol metabolism. The prediction showed that SEC14L2 directly interacts with SCARB1 to regulate cholesterol metabolism (Fig. 4B). Subsequently, the expression of cholesterol

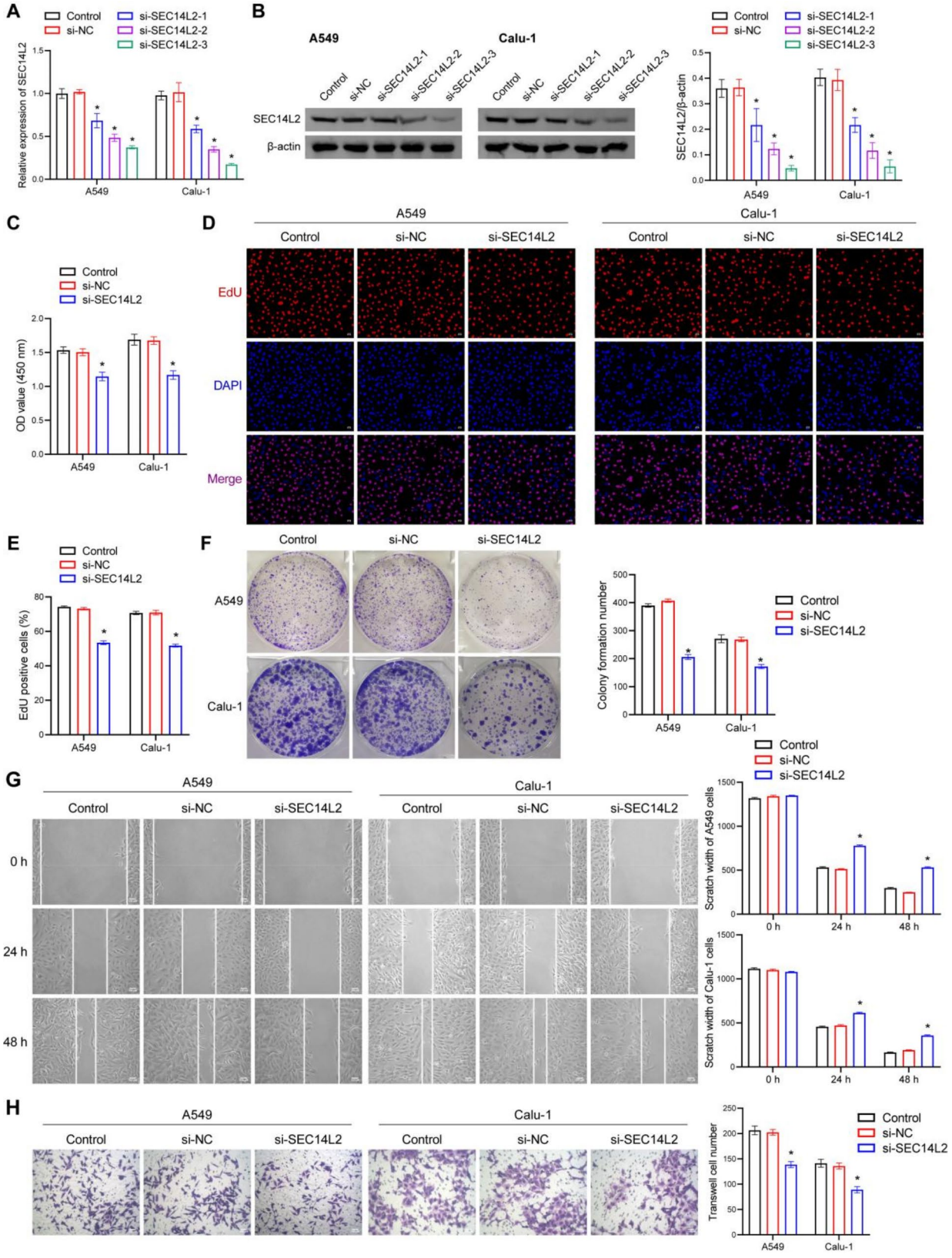

Fig. 2 The inhibition of SEC14L2 expression suppressed the proliferation and migration of A549 and Calu-1 cells. (**A** and **B**) si-SEC14L2-1, si-SEC14L2-2, si-SEC14L2-3 and si-NC were transfected into A549 and Calu-1 cells, SEC14L2 expression was detected using RT-qPCR and WB. (**C**) CCK-8 assay was used to assess the viability of A549 and Calu-1 cells. (**D**-**F**) Cell proliferation was evaluated using EdU and colony formation assays. (**G** and **H**) The wound-healing and transwell assay were used to detect cell migration ability. **P* < 0.05 vs. si-NC

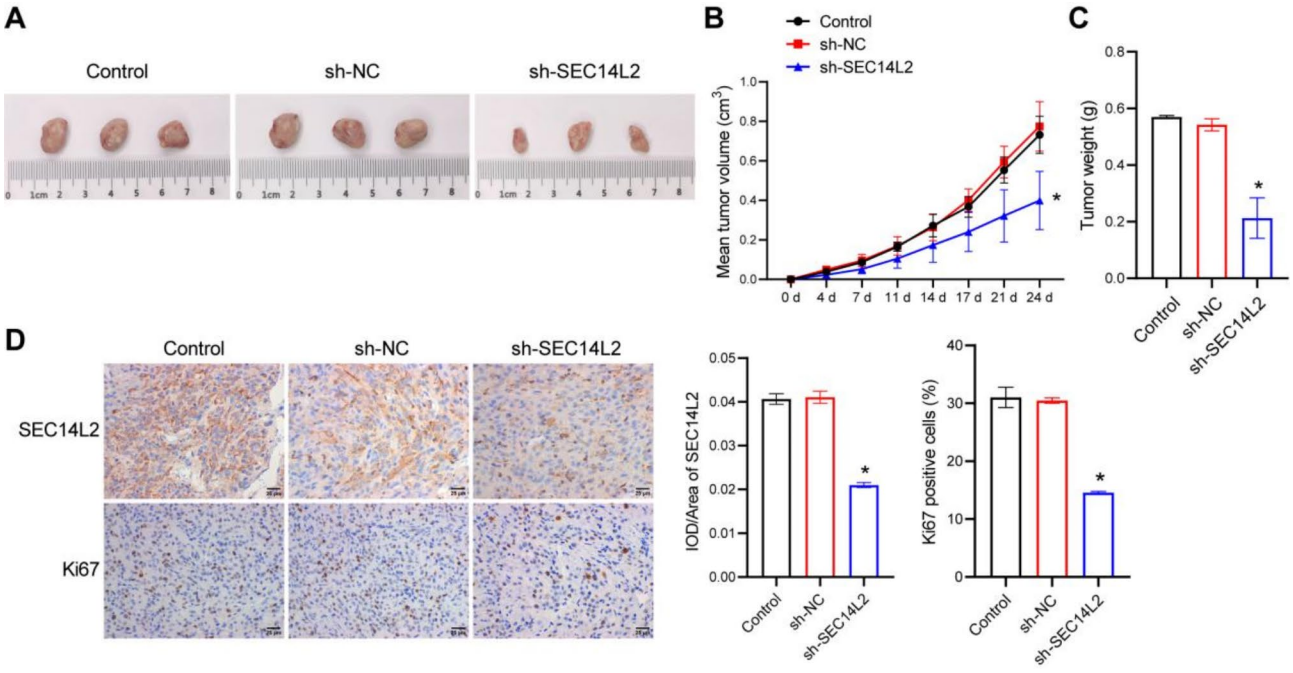

Fig. 3 SEC14L2 promoted the development of NSCLC. (**A-C**) Tumor formation experiments were used to measure tumor size, growth, and weight. (**D**) IOD/Area of SEC14L2 and Ki67 positive cells were detected by IHC. *$P < 0.05$ vs. sh-NC

transport-related indicators was detected using WB. As described in Fig. 4C, the expression of cholesterol uptake-related proteins LDLR and SCARB1 was significantly decreased in the sh-SEC14L2 group compared with the sh-NC group. However, the expression of cholesterol efflux-related protein ABCA1 did not exhibit significant changes. In addition, we also used related kits to detect the cholesterol content in tumors. The results demonstrated that the cholesterol content in tumors was significantly reduced after knocking down SEC14L2 (Fig. 4D). In order to further explore the impact of SEC14L2 on cholesterol uptake in A549 and Calu-1 cells, we supplemented the cells with cholesterol. WB results showed that the expressions of LDLR and SCARB1 were notably diminished in both A549 and Calu-1 cells following silencing SEC14L2, while there were no significant changes in the expression of ABCA1 (Fig. 4E). At the same time, the cholesterol content was significantly reduced (Fig. 4F). To make the comparison of results significant, we first subjected cells to cholesterol depletion followed by cholesterol rescue. After the intervention with MβCD-chol, the intracellular cholesterol content of A549 and Calu-1 cells showed a significant increase. On this basis, knocking down the expression of SEC14L2 found that the intracellular cholesterol content was significantly reduced (Fig. 4G). In order to further confirm the regulatory relationship between SEC14L2 and SCARB1, IF co-localization was applied to analyze the spatial localization of SEC14L2 and SCARB1 (Fig. 4H and I). Co-IP results provided evidence of an interaction between SEC14L2 and SCARB1 (Fig. 4J). These results indicated that SEC14L2 targeted SCARB1 to regulate cholesterol uptake in A549 and Calu-1 cell lines.

SEC14L2 regulated cholesterol metabolism through SCARB1

To investigate the role of SCARB1 in cholesterol metabolism, A549 and Calu-1 cells were treated with MβCD-chol and transfected with si-SCARB1 and oe-SCARB1 and their negative control. The RT-qPCR and WB results verified the success of cell transfection (Figure S1). Subsequently, we examined the cholesterol content of the cells in each treatment group. Compared with the MβCD-chol+si-NC group, the cholesterol levels in the MβCD-chol+si-SCARB1 group were significantly decreased. Then, the cholesterol levels in the MβCD-chol+oe-SCARB1 group were significantly increased compared with the MβCD-chol+oe-NC group (Fig. 5A). These results showed that SCARB1 positively regulated cholesterol levels in A549 and Calu-1 cells. Moreover, overexpression of SCARB1 partially counteracted the inhibitory effect of silencing SEC14L2 on cholesterol intake. Conversely, silencing SCARB1 partially attenuated the promoting effect of overexpressing SEC14L2 on cholesterol intake (Fig. 5B and C). In conclusion, our results suggested that SEC14L2 participates in cholesterol metabolism by regulating SCARB1.

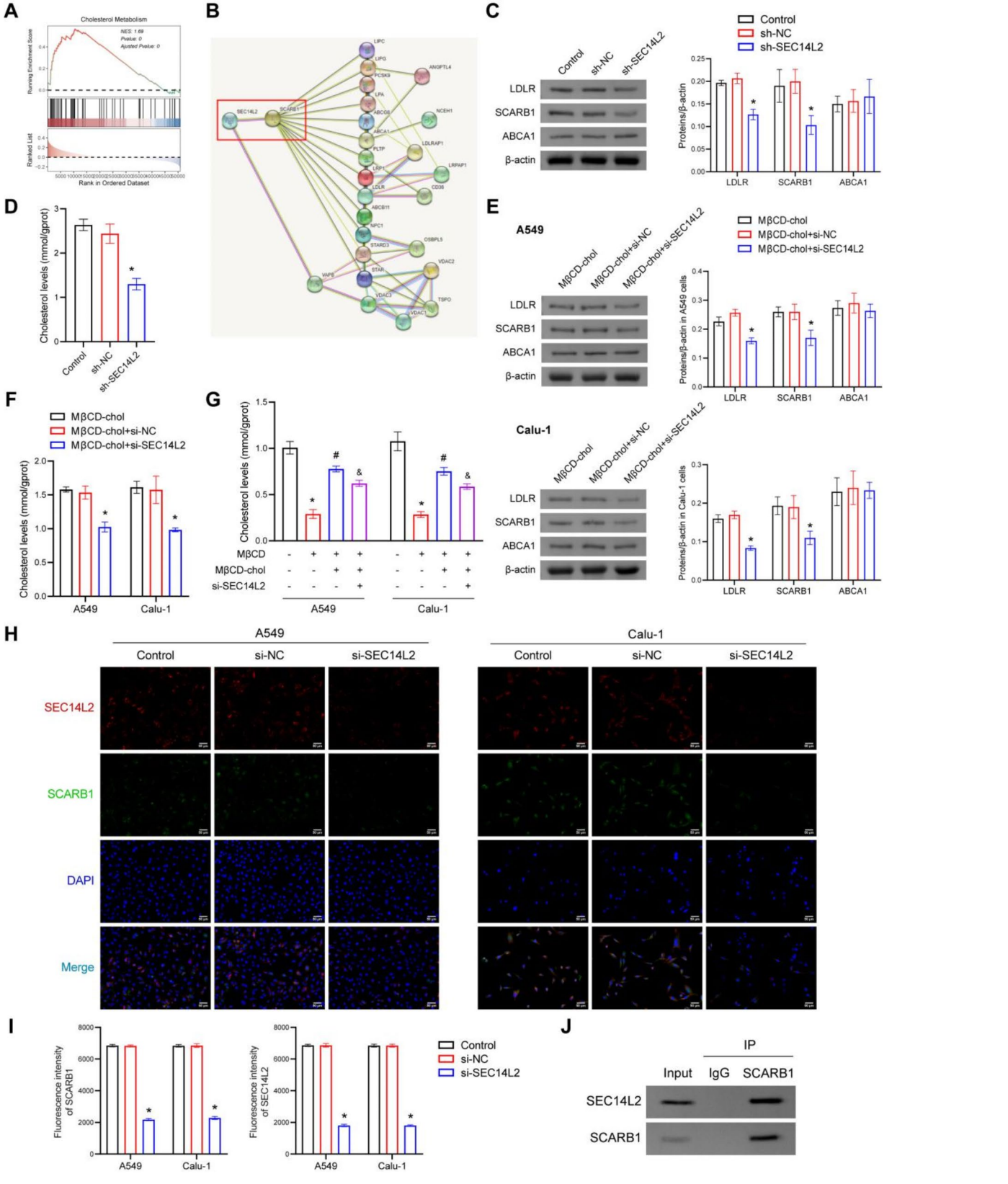

Fig. 4 (See legend on next page.)

(See figure on previous page.)

Fig. 4 SEC14L2 targets SCARB1 to regulate cholesterol uptake. (**A**) GSEA analysis was used to enrich functional pathways of the SEC14L2 gene. (**B**) STRING predicted the protein-protein interaction between SEC14L2 and SCARB1. (**C**) The expressions of cholesterol transport-related proteins LDLR, SCARB1, and ABCA1 were detected by WB. (**D**) The cholesterol content in the tumor was detected by a cholesterol detection kit. *$P < 0.05$ vs. sh-NC. (**E** and **F**) WB and the kit were used to detect the expressions of LDLR, SCARB1, ABCA1, and cholesterol content, respectively. *$P < 0.05$ vs. MβCD-chol + si-NC. (**G**) The content of cholesterol in A549 and Calu-1 cells after cholesterol depletion was detected using the kit. *$P < 0.05$ vs. Control, #$P < 0.05$ vs. MβCD, &$P < 0.05$ vs. MβCD + MβCD-chol. (**H** and **I**) The spatial localization of SEC14L2 and SCARB1 was analyzed by IF. *$P < 0.05$ vs. si-NC. (**J**) Co-IP was used to confirm the targeting relationship between SEC14L2 and SCARB1

Discussion

Cholesterol is a crucial lipid constituent in mammalian cell membranes, which could maintain the integrity and fluidity of the cell membrane. It also contributes to the formation of the microstructure of the cell membrane [28, 29]. The role of dietary cholesterol and high serum cholesterol in cancer is still controversial. Studies reported that high serum cholesterol levels increase natural killer cells' antitumor function and reduce mouse liver tumor growth [30]. However, other studies demonstrated the contribution of intracellular cholesterol accumulation to tumor formation or growth [31, 32]. Firstly, we conducted bioinformatics analysis to identify differentially expressed genes related to cholesterol metabolism and selected SEC14L2 as the key gene for this study. Subsequently, we conducted both in vitro and in vivo experiments to verify our findings, demonstrating that SEC14L2 promoted cholesterol uptake in NSCLC cells, which promoted NSCLC development.

In this study, we identified the cholesterol metabolic-related gene SEC14L2 as a high-risk gene by Cox and survival analysis. Specifically, our findings revealed a significant difference in survival rates between the low-expression and high-expression groups, with the former exhibiting a notably higher survival rate. Therefore, we hypothesized that SEC14L2 could promote the growth of NSCLC cells. We further showed that silencing SEC14L2 inhibited cell proliferation and migration and suppressed the tumorigenic potential of A549 cells in nude mice. However, SEC14L2 seemed to play different roles in different tumor cells. In a study conducted by Li et al., it was demonstrated that SEC14L2 played an inhibitory role in the proliferation of liver cancer cells. Further, significant inhibition of tumor growth was observed in mouse models [18]. Additionally, silencing SEC14L2 was found to promote cell proliferation, migration, invasion, and cell cycle progression in castration-resistant prostate cancer cells. It was related to the invasiveness and poor prognosis of prostate cancer [17]. These results suggested that SEC14L2 could be both a tumor promoter and suppressor.

The intracellular balance of cholesterol metabolism is tightly controlled through a complex network that governs processes such as cholesterol biosynthesis, uptake, efflux, conversion, esterification, and transport [33, 34]. However, tumor cells exhibited abnormal cholesterol metabolism to meet the high energy and biosynthetic requirements associated with rapid growth [35]. Therefore, strategies to reduce cholesterol synthesis or inhibit cholesterol uptake were suggested as potential antitumor therapies [36, 37]. In our study, GSEA enrichment analysis revealed that the low expression phenotype of SEC14L2 was mainly concentrated in the cholesterol metabolism pathway. Moreover, silencing of SEC14L2 inhibited the expression of cholesterol uptake-related proteins LDLR and SCARB1 but had no significant effect on cholesterol efflux-related protein ABCA1. These results indicated that SEC14L2 might affect cholesterol uptake in NSCLC cells. In addition, studies showed that some tumor cells were more inclined to sacrifice synthetic pathways to avoid consuming ATP during biosynthesis [35]. Otherwise, abundant exogenous cholesterol could be obtained by promoting the expression of lipoprotein receptors such as LDLR and SCARB1 [38]. In humans, several SNPs in the SCARB1 gene were found to affect cholesterol metabolism and fertility [39]. SCARB1 was essential for cholesterol uptake, and blocking SCARB1 led to clear cell renal cell carcinoma cell-cycle arrest and apoptosis [20]. Skin cutaneous melanoma exhibited SCARB1-mediated cholesterol-dependent metabolism [21]. Moreover, previous studies reported that SCARB1 was closely related to the development of cancer. SCARB1 was positively associated with metastasis and poor prognosis of nasopharyngeal carcinoma [40]. SCARB1 exhibited high expression levels in specific subsets of lung large-cell carcinoma and small-cell lung cancer patients. Further investigations revealed that inhibition of SCARB1 expression effectively suppressed the growth of lung cancer cells [41]. Our study represented the first report on the involvement of SCARB1 in regulating cholesterol metabolism in NSCLC.

However, some limitations should be acknowledged in this study. Firstly, the results of our study were based on NSCLC cell lines and nude mouse models, which might not fully reflect the complexity and dynamic characteristics of human NSCLC patients. Therefore, it was necessary to include human samples or clinical data. Secondly, due to the lack of animal models overexpressing or knocking out SEC14L2, the functional characterization of SEC14L2 in vivo was challenging. The lack of specific activators for the SEC14L2/SCARB1 signaling pathway also hindered a comprehensive understanding of how SEC14L2 regulated these pathways in vitro and in vivo. By addressing these issues, the reliability and

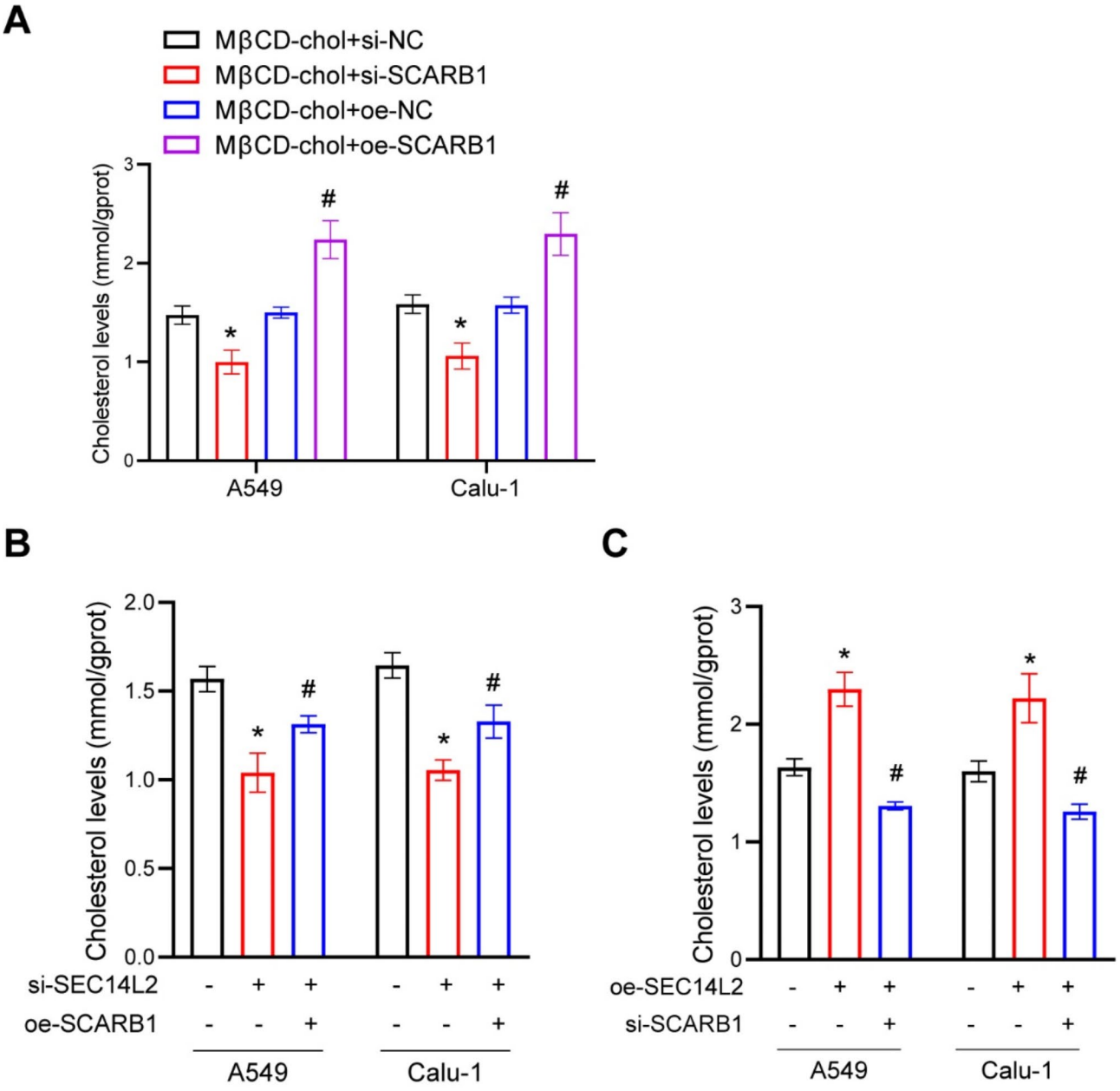

Fig. 5 SEC14L2 regulated cholesterol metabolism through SCARB1. (**A-C**) The intracellular cholesterol content was detected by the kit. *$P < 0.05$ vs. MβCD-chol + si-NC or MβCD-chol + si-NC + oe-NC, #$P < 0.05$ vs. MβCD-chol + oe-NC or MβCD-chol + si-SEC14L2 + oe-NC

persuasiveness of the research can be further improved, leading to a better understanding of the role and mechanisms of SEC14L2 in NSCLC.

Conclusion

The present study revealed SEC14L2 as a crucial gene in predicting the prognosis of NSCLC patients. It validated SEC14L2 as a potential tumor-promoting gene in NSCLC in vitro and in vivo. Therefore, we could inhibit the cholesterol uptake of NSCLC cells by silencing the SEC14L2/SCARB1 signaling pathway, thereby suppressing NSCLC development. Our findings suggested that SEC14L2 could serve as a promising therapeutic target for NSCLC.

Abbreviations

NSCLC	Non-small cell lung cancer
SEC14L2	Sect. 14-like lipid binding 2
CCK-8	Cell Counting Kit-8
IHC	Immunohistochemistry
MβCD	Methyl-β-cyclodextrin
LDLR	Low-density lipoprotein receptor
SCARB1	Scavenger receptor class B member 1

Supplementary Information

The online version contains supplementary material available at https://doi.org/10.1186/s12944-024-02401-9.

Supplementary Material 1: **Figure S1.** After silencing SCARB1 and overexpressing SCARB1 in A549 and Calu-1 cells, (A) SCARB1 mRNA expression was detected by RT-qPCR; (B) WB was used to detect SCARB1 protein expression. **P* < 0.05 vs. si-NC, #*P* < 0.05 vs. oe-NC.

Supplementary Material 2

Author contributions

Q.Z. contributions to data curation, investigation, validation, writing of the original draft. D.L. contributed to investigation, software and validation. Yanchao.L. contributed to formal analysis and methodology. Yunzhu.L. and Yi.L. contributed to conceptualization, funding acquisition, project administration, supervision, and review. All authors read and approved the final manuscript.

Funding

This work was supported by the Natural Science Foundation of Hunan Province (No. 2022JJ50105).

Data availability

No datasets were generated or analysed during the current study.

Declarations

Ethics approval and consent to participate

All experimental procedures and animal handling were performed with the approval of the Animal Care and Use Committee of the Second Xiangya Hospital, Central South University (Approval No. 2023867), in accordance with the National Institutes of Health Guide for the Care and Use of Laboratory Animals, and studies involving laboratory animals follows the ARRIVE guidelines.

Competing interests

The authors declare no competing interests.

Received: 25 July 2024 / Accepted: 9 December 2024
Published online: 18 December 2024

References

1. Siegel RL, Miller KD, Fuchs HE, Jemal A. Cancer statistics, 2022. CA Cancer J Clin. 2022;72:7–33. https://doi.org/10.3322/caac.21708.
2. Chen P, Liu Y, Wen Y, Zhou C. Non-small cell lung cancer. China Cancer Commun (Lond). 2022;42:937–70. https://doi.org/10.1002/cac2.12359.
3. Liu VN, Zuniga KB, Paciorek A, Zhang L, Chan JM, Carroll PR, et al. Barriers and confidence among colorectal and prostate cancer survivors participating in two behavioral intervention studies. Support Care Cancer. 2023;31:453. https://doi.org/10.1007/s00520-023-07901-5.
4. Surwillo A, Wawrzyniak A. Nutritional assessment of selected patients with cancer. Rocz Panstw Zakl Hig. 2013;64:225–33.
5. Kuzu OF, Noory MA, Robertson GP. The role of cholesterol in Cancer. Cancer Res. 2016;76:2063–70. https://doi.org/10.1158/0008-5472.Can-15-2613.
6. Fessler MB. We need to talk about lung cancer's cholesterol-hoarding problem. Cell Stem Cell. 2023;30:745–7. https://doi.org/10.1016/j.stem.2023.05.006.
7. Ben Hassen C, Goupille C, Vigor C, Durand T, Guéraud F, Silvente-Poirot S, et al. Is cholesterol a risk factor for breast cancer incidence and outcome? J Steroid Biochem Mol Biol. 2023;232:106346. https://doi.org/10.1016/j.jsbmb.2023.106346.
8. Tibbo AJ, Hartley A, Vasan R, Shaw R, Galbraith L, Mui E, et al. MBTPS2 acts as a regulator of lipogenesis and cholesterol synthesis through SREBP signalling in prostate cancer. Br J Cancer. 2023;128:1991–9. https://doi.org/10.1038/s41416-023-02237-7.
9. Deng W, Liu H, Luo S, Clarke J, Glass C, Su L, et al. APOB genotypes and CDH13 haplotypes in the cholesterol-related pathway genes predict Non-small Cell Lung Cancer Survival. Cancer Epidemiol Biomarkers Prev. 2020;29:1204–13. https://doi.org/10.1158/1055-9965.Epi-19-1262.
10. Kim H, Choi SY, Lim J, Lindroth AM, Park YJ. EHMT2 inhibition induces cell death in Human Non-small Cell Lung Cancer by altering the cholesterol biosynthesis pathway. Int J Mol Sci. 2020;21. https://doi.org/10.3390/ijms21031002.
11. Hsu JL, Leu WJ, Zhong NS, Guh JH. Autophagic activation and decrease of plasma membrane cholesterol contribute to Anticancer activities in Non-small Cell Lung Cancer. Molecules. 2021;26. https://doi.org/10.3390/molecules26195967.
12. Mohammadalipour A, Showalter CA, Muturi HT, Farnoud AM, Najjar SM, Burdick MM. Cholesterol depletion decreases adhesion of non-small cell lung cancer cells to E-selectin. Am J Physiol Cell Physiol. 2023;325:C471–82. https://doi.org/10.1152/ajpcell.00197.2020.
13. Guilbaud E, Barouillet T, Ilie M, Borowczyk C, Ivanov S, Sarrazy V, et al. Cholesterol efflux pathways hinder KRAS-driven lung tumor progenitor cell expansion. Cell Stem Cell. 2023;30:800–e817809. https://doi.org/10.1016/j.stem.2023.05.005.
14. Zingg JM, Libinaki R, Meydani M, Azzi A. Modulation of phosphorylation of tocopherol and phosphatidylinositol by hTAP1/SEC14L2-mediated lipid exchange. PLoS ONE. 2014;9:e101550. https://doi.org/10.1371/journal.pone.0101550.
15. Costa R, Todt D, Zapatero-Belinchón F, Schenk C, Anastasiou OE, Walker A, et al. SEC14L2, a lipid-binding protein, regulates HCV replication in culture with inter- and intra-genotype variations. J Hepatol. 2019;70:603–14. https://doi.org/10.1016/j.jhep.2018.11.012.
16. Zingg JM, Azzi A, Meydani M. Induction of VEGF expression by alpha-tocopherol and alpha-tocopheryl phosphate via PI3Kγ/PKB and hTAP1/SEC14L2-mediated lipid exchange. J Cell Biochem. 2015;116:398–407. https://doi.org/10.1002/jcb.24988.
17. Liu S, Huang D, Huang J, Yan J, Chen T, Zhang N, et al. Genome-wide expression analysis identifies the association between SEC14L2 and castration-resistant prostate Cancer Survival. J Cancer. 2021;12:2173–80. https://doi.org/10.7150/jca.50299.
18. Li Z, Lou Y, Tian G, Wu J, Lu A, Chen J, et al, et al. Discovering master regulators in hepatocellular carcinoma: one novel MR, SEC14L2 inhibits cancer cells. Aging. 2019;11:12375–411. https://doi.org/10.18632/aging.102579.
19. Geiger T, Madden SF, Gallagher WM, Cox J, Mann M. Proteomic portrait of human breast cancer progression identifies novel prognostic markers. Cancer Res. 2012;72:2428–39. https://doi.org/10.1158/0008-5472.Can-11-3711.
20. Riscal R, Bull CJ, Mesaros C, Finan JM, Carens M, Ho ES, et al. Cholesterol auxotrophy as a Targetable vulnerability in Clear Cell Renal Cell Carcinoma. Cancer Discov. 2021;11:3106–25. https://doi.org/10.1158/2159-8290.Cd-21-0211.
21. Song L, Wang S, Zhang X, Song N, Lu Y, Qin C. Bridging the gap between clear cell renal cell carcinoma and cutaneous melanoma: the role of SCARB1 in dysregulated cholesterol metabolism. Aging. 2023;15:10370–88. https://doi.org/10.18632/aging.205083.
22. Du Y, Miao W, Jiang X, Cao J, Wang B, Wang Y, et al. The epithelial to mesenchymal transition related Gene Calumenin is an adverse prognostic factor of bladder Cancer correlated with Tumor Microenvironment Remodeling, Gene Mutation, and Ferroptosis. Front Oncol. 2021;11:683951. https://doi.org/10.3389/fonc.2021.683951.
23. Liang G, Meng W, Huang X, Zhu W, Yin C, Wang C, et al. miR-196b-5p-mediated downregulation of TSPAN12 and GATA6 promotes tumor progression in non-small cell lung cancer. Proc Natl Acad Sci U S A. 2020;117:4347–57. https://doi.org/10.1073/pnas.1917531117.
24. Yang T, Li H, Chen T, Ren H, Shi P, Chen M. LncRNA MALAT1 Depressed Chemo-Sensitivity of NSCLC cells through directly functioning on miR-197-3p/p120 catenin Axis. Mol Cells. 2019;42:270–83. https://doi.org/10.14348/molcells.2019.2364.
25. Ma Y, Kang B, Li S, Xie G, Bi J, Li F, et al. CRISPR-mediated MECOM depletion retards tumor growth by reducing cancer stem cell properties in lung squamous cell carcinoma. Mol Ther. 2022;30:3341–57. https://doi.org/10.1016/j.ymthe.2022.06.011.
26. Zheng S, Lin J, Pang Z, Zhang H, Wang Y, Ma L, et al. Aberrant cholesterol metabolism and Wnt/β-Catenin signaling Coalesce via Frizzled5 in supporting Cancer Growth. Adv Sci (Weinh). 2022;9:e2200750. https://doi.org/10.1002/advs.202200750.

27. Tang CT, Yang J, Liu ZD, Chen Y, Zeng C. Taraxasterol acetate targets RNF31 to inhibit RNF31/p53 axis-driven cell proliferation in colorectal cancer. Cell Death Discov. 2021;7:66. https://doi.org/10.1038/s41420-021-00449-5.
28. Espinosa G, López-Montero I, Monroy F, Langevin D. Shear rheology of lipid monolayers and insights on membrane fluidity. Proc Natl Acad Sci U S A. 2011;108:6008–13. https://doi.org/10.1073/pnas.1018572108.
29. Xiao M, Xu J, Wang W, Zhang B, Liu J, Li J, et al. Functional significance of cholesterol metabolism in cancer: from threat to treatment. Exp Mol Med. 2023;55:1982–95. https://doi.org/10.1038/s12276-023-01079-w.
30. Qin WH, Yang ZS, Li M, Chen Y, Zhao XF, Qin YY, et al. High serum levels of cholesterol increase Antitumor functions of Nature Killer cells and reduce growth of liver tumors in mice. Gastroenterology. 2020;158:1713–27. https://doi.org/10.1053/j.gastro.2020.01.028.
31. Ma X, Bi E, Lu Y, Su P, Huang C, Liu L, et al. Cholesterol induces CD8(+) T cell exhaustion in the Tumor Microenvironment. Cell Metab. 2019;30:143–e156145. https://doi.org/10.1016/j.cmet.2019.04.002.
32. Krycer JR, Brown AJ. Cholesterol accumulation in prostate cancer: a classic observation from a modern perspective. Biochim Biophys Acta. 2013;1835:219–29. https://doi.org/10.1016/j.bbcan.2013.01.002.
33. Luo J, Yang H, Song BL. Mechanisms and regulation of cholesterol homeostasis. Nat Rev Mol Cell Biol. 2020;21:225–45. https://doi.org/10.1038/s41580-019-0190-7.
34. Cardoso D, Perucha E. Cholesterol metabolism: a new molecular switch to control inflammation. Clin Sci (Lond). 2021;135:1389–408. https://doi.org/10.1042/cs20201394.
35. Xu H, Zhou S, Tang Q, Xia H, Bi F. Cholesterol metabolism: new functions and therapeutic approaches in cancer. Biochim Biophys Acta Rev Cancer. 2020;1874:188394. https://doi.org/10.1016/j.bbcan.2020.188394.
36. Guillaumond F, Bidaut G, Ouaissi M, Servais S, Gouirand V, Olivares O, et al. Cholesterol uptake disruption, in association with chemotherapy, is a promising combined metabolic therapy for pancreatic adenocarcinoma. Proc Natl Acad Sci U S A. 2015;112:2473–8. https://doi.org/10.1073/pnas.1421601112.
37. Ding X, Zhang W, Li S, Yang H. The role of cholesterol metabolism in cancer. Am J Cancer Res. 2019;9:219–27.
38. Traughber CA, Opoku E, Brubaker G, Major J, Lu H, Lorkowski SW, et al. Uptake of high-density lipoprotein by scavenger receptor class B type 1 is associated with prostate cancer proliferation and tumor progression in mice. J Biol Chem. 2020;295:8252–61. https://doi.org/10.1074/jbc.RA120.013694.
39. Casado ME, Huerta L, Marcos-Díaz A, Ortiz AI, Kraemer FB, Lasunción MA, et al. Hormone-sensitive lipase deficiency affects the expression of SR-BI, LDLr, and ABCA1 receptors/transporters involved in cellular cholesterol uptake and efflux and disturbs fertility in mouse testis. Biochim Biophys Acta Mol Cell Biol Lipids. 2021;1866:159043. https://doi.org/10.1016/j.bbalip.2021.159043.
40. Chen W, Bao L, Ren Q, Zhang Z, Yi L, Lei W, et al. SCARB1 in extracellular vesicles promotes NPC metastasis by co-regulating M1 and M2 macrophage function. Cell Death Discov. 2023;9:323. https://doi.org/10.1038/s41420-023-01621-9.
41. Kato T, Lee D, Huang H, Cruz W, Ujiie H, Fujino K, et al. Personalized siRNA-Nanoparticle systemic therapy using metastatic lymph node specimens obtained with EBUS-TBNA in Lung Cancer. Mol Cancer Res. 2018;16:47–57. https://doi.org/10.1158/1541-7786.Mcr-16-0341.

Publisher's note